



**HAL**  
open science

## Role of Underlayer for Efficient Core–Shell InGaN QWs Grown on m-plane GaN Wire Sidewalls

Akanksha Kapoor, Sylvain Finot, Vincent Grenier, Eric Robin, Catherine Bougerol, Joël Bleuse, Gwenolé Jacopin, J. Eymery, Christophe Durand

► **To cite this version:**

Akanksha Kapoor, Sylvain Finot, Vincent Grenier, Eric Robin, Catherine Bougerol, et al.. Role of Underlayer for Efficient Core–Shell InGaN QWs Grown on m-plane GaN Wire Sidewalls. *ACS Applied Materials & Interfaces*, 2020, 12 (16), pp.19092-19101. 10.1021/acsami.9b19314 . cea-02540566

**HAL Id: cea-02540566**

**<https://cea.hal.science/cea-02540566>**

Submitted on 10 Nov 2020

**HAL** is a multi-disciplinary open access archive for the deposit and dissemination of scientific research documents, whether they are published or not. The documents may come from teaching and research institutions in France or abroad, or from public or private research centers.

L'archive ouverte pluridisciplinaire **HAL**, est destinée au dépôt et à la diffusion de documents scientifiques de niveau recherche, publiés ou non, émanant des établissements d'enseignement et de recherche français ou étrangers, des laboratoires publics ou privés.

## **Role of underlayer for efficient core-shell InGaN QWs grown on *m*-plane GaN wire sidewalls**

Akanksha Kapoor,<sup>\*†</sup> Sylvain Finot,<sup>‡</sup> Vincent Grenier,<sup>†</sup> Eric Robin,<sup>§</sup> Catherine Bougerol,<sup>‡</sup> Joel Bleuse,<sup>†</sup> Gwénoél Jacopin,<sup>‡</sup> Joël Eymery,<sup>§</sup> and Christophe Durand<sup>\*†</sup>

<sup>†</sup>Univ. Grenoble Alpes, CEA, IRIG, PHELIQS, NPSC, Grenoble 38000, France

<sup>‡</sup>Univ. Grenoble Alpes, CNRS, Institut Néel, Grenoble 38000, France

<sup>§</sup>Univ. Grenoble Alpes, CEA, IRIG, MEM, LEMMA, Grenoble 38000, France

<sup>§</sup>Univ. Grenoble Alpes, CEA, IRIG, MEM, NRS, Grenoble 38000, France

a) Authors to whom correspondence should be addressed: [akanksha.kapoor@cea.fr](mailto:akanksha.kapoor@cea.fr),  
[christophe.durand@cea.fr](mailto:christophe.durand@cea.fr)

## ABSTRACT

Different types of buffer layers like InGaN underlayer (UL) and InGaN/GaN superlattices are now well-known to significantly improve the efficiency of *c*-plane InGaN/GaN based light emitting diodes (LEDs). The present work investigates the role of two different kinds of pre-growth layers (low In-content InGaN UL and GaN UL namely “GaN spacer”) on the emission of core-shell *m*-plane InGaN/GaN single quantum well (QW) grown around Si-doped  $\bar{c}$ -GaN microwires obtained by silane-assisted MOVPE. According to photo- and cathodoluminescence measurements performed at room temperature, an improved efficiency of light emission at 435 nm with internal quantum efficiency > 15 % has been achieved by adding a GaN spacer prior to the growth of QW. As revealed by scanning transmission electron microscopy, an ultra-thin residual layer containing Si located at the wire sidewall surfaces favors the formation of high-density of extended defects nucleated at the first InGaN QW. This contaminated residual incorporation is buried by the growth of GaN spacer and avoids the structural defect formation, therefore explaining the improved optical efficiency. No further improvement is observed by adding the InGaN UL to the structure, which is confirmed by comparable values of the effective carrier lifetime estimated from time-resolved (TR) experiments. Contrary to the case of planar *c*-plane QW where the improved efficiency is attributed to a strong decrease of point defects, the addition of an InGaN UL seem to have no influence in the case of radial *m*-plane QW.

**Keywords:** Nanowires, GaN, MOVPE, nitride semiconductors, InGaN, quantum wells

## INTRODUCTION

Blue planar *c*-plane GaN light emitting diodes (LEDs) comprising several InGaN quantum wells (QWs) with indium content in the range of 15-18% can be achieved with an external quantum efficiency higher than 80%,<sup>1,2</sup> yet these conventional devices suffer adversely from the efficiency droop at high current injection. Further, the structures grown along the *c*-axis are negatively affected by quantum confined stark effect (QCSE),<sup>3</sup> which hinders the radiative efficiency of the InGaN/GaN LEDs and also results in a longer carrier lifetime thus limiting their use in visible light communication (VLC) devices. During the last decade, core-shell InGaN/GaN QWs grown on GaN nanowires have been intensely studied<sup>4,5,6,7,8,9</sup> in order to overcome the limitations of planar structures. Nanowire geometry is an important area of investigation for LED application and presents key-advantages such as the growth of radial non-polar *m*-plane QWs to avoid QCSE,<sup>4</sup> a high tolerance to lattice mismatched substrates (such as silicon<sup>10</sup> or sapphire<sup>11</sup>) with an intrinsic low density of dislocations along the wires<sup>12,13</sup> a large increase of active region area limiting the droop efficiency thanks to the reduction of the current density.<sup>14</sup> Such core-shell wires can also be used to develop flexible devices (LEDs and photodetectors)<sup>15,16,17,18</sup> and GHz-range  $\mu$ -LEDs for VLC applications due to the reduced carrier lifetimes of *m*-plane non-polar InGaN QWs.<sup>19</sup> However, despite the expected QCSE mitigation and dislocation-free crystal quality, the internal quantum efficiency (IQE) measured by temperature-dependence photoluminescence is generally found in the range of 5-20% for *m*-plane core-shell InGaN multiple quantum wells (MQWs) emitting blue light.<sup>20,14</sup> These efficiencies still remain low in comparison of standard planar LEDs. Combining with high-efficient phosphors, white wires based-LED have been achieved with relatively low external quantum efficiency (EQE): 3% has been reported for Ga-polar blue-emitting InGaN/GaN core-shell micro rod LED<sup>8</sup> at a current

density of 40 A/cm<sup>2</sup>, while 12.5% of EQE of has been reported from N-polar radial InGaN/GaN core-shell wires<sup>15</sup> at a current density of 14 A/cm<sup>2</sup>.

Several researcher and industrial groups have made effort to improve the efficiency of such core-shell wire-LEDs. The addition of AlGaN underlayer (UL) on core-shell InGaN/GaN MQWs has recently been studied showing an improvement of IQE from 29 to 35%.<sup>21,22</sup> Also, Rishinaramangalam *et al.* demonstrated a reduction of reverse leakage current on wires and triangular stripes covered with InGaN MQWs in presence of AlGaN UL.<sup>23</sup> A further optimized core-shell LED structure including AlGaN UL and electron blocking barrier (EBL) exhibiting an IQE as high as 62% have been reported by the group of Feezell with the demonstration wire-LED having an EQE equal to 8.3%.<sup>19,24</sup> Also, the group of Waag and the company Osram report core-shell wire-LED with high IQE (about 60%) and high EQE (maximum of 10% at current density of 40 A/cm<sup>2</sup>).<sup>25</sup> Therefore, achieving high efficiency with wire-based LED remains a significant challenge till date to be able to compete against the present planar technology.

The high efficiency of standard *c*-planar LEDs corresponds to extensive research efforts during more two decades. Among all strategies to raise the efficiency, the use of underlayers (ULs) can exhibit impressive enhancement of efficiency in InGaN/GaN MQW structures by exploiting different types of buffer layers in InGaN/GaN structures such as short-period InGaN/GaN superlattices,<sup>26,27</sup> Si-doped (In)GaN prelayers<sup>28</sup> and InGaN underlayer (UL) with low In-content.<sup>29,30,31,32</sup> A recent investigation about the role of InGaN underlayer to increase the InGaN/GaN QW efficiency reveals that an optimized thickness of 55 nm with around 3% indium content significantly improves the EQE by 3.5 times,<sup>32</sup> while at room temperature the QW effective lifetime increases from 170 ps (no UL present) to 20 ns (with UL) indicating a low non-radiative (NR) recombination rate.<sup>33</sup> According to the proposed mechanism, the NR centers

corresponds to the GaN surface point defects created by the high-temperature growth of GaN prior to QW. They are then trapped by the InGaN UL allowing a later defect-free QW growth.<sup>33</sup> Apart from utilizing InGaN UL as a buffer layer, some recent work also demonstrates that GaN buffer layer grown at low temperature under nitrogen improves the PL emission (by 40%) by suppressing some QW chemical contaminations, as indicated by SIMS analysis.<sup>34</sup> In view of the remarkable improvement in the *c*-plane QW efficiency by inserting the buffer layers, it could be interesting to extend this strategy to *m*-plane core-shell heterostructures. Because the surface energy of GaN differs from *c*-plane to *m*-plane, a variation in the defect density for the InGaN QW grown on the two different facets can be expected. For instance, the additional AlGaIn UL have been successfully integrated in core-shell InGaIn QWs allowing to improve the IQE and EQE of wire-LEDs, as previously mentioned.<sup>21,22,23,24</sup>

Hence, the objective of this work is to extend the UL study of *m*-plane core-shell InGaIn MQW systems investigating the influence of GaN and low In-content InGaIn pre-growth layers in order to improve the QW luminescence efficiency. The pre-growth of GaN layer aims to improve the crystal structural quality before the QW growth (GaN pre-layer is called “GaN spacer” hereafter). In addition to this first building block, the growth of an additional low In-content InGaIn layer is performed expecting a reduction of point defects (as reported in the literature for *c*-plane surfaces) to improve the QW efficiency (this additional layer is called “InGaIn UL”). In order to study the impact of these two types of pre-layers, we propose to work on a simple system composed of GaN wires with a core-shell InGaIn single quantum well (SQW) exhibiting blue emission. A careful investigation combining both structural and optical measurements for the wires is presented. Photoluminescence (PL) and cathodoluminescence (CL) are performed at room temperature to study the spatial emission from wires, while time-resolved (TR)

measurement including TRCL and TRPL provide insights of carriers' recombination along with an estimation of internal quantum efficiency (IQE) variation. A detailed discussion including structural analyses by scanning transmission electron microscopy (STEM) is proposed to understand the results.

## EXPERIMENTAL SECTION

Self-assembled GaN wires are grown on nitridated *c*-plane sapphire substrates along the  $\bar{c}$ -direction (i.e. N-polar) by catalyst-free metal organic vapor phase epitaxy (MOVPE) using silane addition in a close coupled showerhead reactor. A thin *in situ* SiN<sub>x</sub> film pre-deposited on the substrate is acting as a partial mask for the growth. The wire-geometry is favored by a high silane flux (~200 nmol/min), a low V/III ratio (~50), a high growth temperature (1040°C) and a high pressure (800 mbar).<sup>11</sup> The high silane flux injection for 300 s results in a heavily n<sup>++</sup> doped GaN wire ( $N_d \approx 10^{20} \text{ cm}^{-3}$ )<sup>35,36</sup> about 18  $\mu\text{m}$  in length. Then, the silane addition is switched off and the GaN wire continues to grow for another 300 s with an unintentionally doped part (but with quite strong residual n-type doping in the order of  $10^{18} \text{ cm}^{-3}$ ).<sup>37</sup> This so called 'upper-part' of the wire' is about 12  $\mu\text{m}$  in length. Three different samples are investigated for the present study based on identical wire-geometry as mentioned above (see the schematics in Figure 1). The first sample is prepared by directly growing radially a single InGaN quantum well (SQW) around the GaN core for 80 s under N<sub>2</sub> with thin GaN capping at growth temperature of 750 °C followed by the growth of a GaN barrier at growth temperature of 850 °C for 150 s (sample #1 so-called "SQW", see Figure 1a). Note that the *m*-plane InGaN/GaN QW grows selectively around the unintentionally doped upper-part of the wire due to the SiN<sub>x</sub> passivation layer formed around the bottom-part from the silane addition in the preliminary stage.<sup>38</sup> The second sample (sample #2 so-called

“GaN-spacer+SQW”, see Figure 1b) is grown under N<sub>2</sub> carrier gas by adding a GaN spacer at 900 °C for 100 s around the GaN core before the similar growth of InGaN SQW ~~and GaN barrier~~ as already performed for the first sample followed by a GaN barrier grown at 750°C for 150 s. The third sample (sample #3 named as “GaN-spacer+UL+SQW”) depicted in the Figure 1c is prepared by growing a GaN spacer (similar growth conditions as mentioned above) followed by the growth of an InGaN underlayer (UL) at 800 °C for 900 s (estimated thickness of 150 nm) to target an indium composition around 3-5% so as to be consistent with the work performed for planar based structures. The growth is followed by a 25 nm-thick GaN layer at the same temperature. Then, the structure is completed by the growth of *m*-plane InGaN/GaN SQW ~~and GaN barrier~~ using the previous growth parameters followed by a GaN barrier at 750°C. It is important to mention that the present study is only performed on single InGaN QW, because for the structures having two or more QWs, the first QW itself may act as a buffer layer, thereby altering the direct influence of a GaN spacer or an UL on the overall QW efficiency. In the same way, the growth temperature of the GaN barrier for samples #2 and #3 is set to 750°C to prevent any influence of temperature on QW efficiency.<sup>33</sup>

30°-tilted scanning electron microscopy (SEM) images of the three samples are shown in Figure 1d,e,f respectively. The core-shell geometry located in the upper part of wires is visible for all samples with wires having a diameter in the 0.7-2 μm range and length in the 25-30 μm range. The average wire density is around 10<sup>6</sup> wire/cm<sup>2</sup> and is similar for all samples. The growth of GaN shell performed at lower temperature (900°C) allows to get radial geometry of the heterostructures. The radial growth has similar length for all samples (about one third of total wire length) corresponding to the length of wire upper-part grown without silane. A residual sidewall overgrowth can be observed at the transition region located between the upper and

bottom part of the wires, which is attributed to a non-continuous passivating film of  $\text{SiN}_x$  around the GaN core.<sup>4,6</sup>

## RESULTS AND DISCUSSION

**Optical Characterizations.** To measure the influence of UL and spacer on the SQW emission, optical properties at room temperature of the samples have been investigated using PL of as-grown wires on sapphire and CL of dispersed wires on silicon substrates. The PL experiment is carried out by using a continuous wave doubled solid-state laser to excite the wires at 244 nm with an excitation power density of  $21 \text{ W/cm}^2$ . The signals are analyzed through a 46 cm focal length spectrometer equipped with a 600 grooves/cm grating and detected with a liquid nitrogen cooled charge coupled device (CCD) camera. For CL experiments, the electron beam with an acceleration voltage of 5 kV and the probe current of about 1 nA is used to excite the wires. The resulting CL signal is collected through entrance slit opened at 1 mm by a parabolic mirror and analyzed with a grating monochromator equipped with a Peltier cooled CCD camera ( $-60 \text{ }^\circ\text{C}$ ).

The PL emission for the three samples recorded strictly in the same conditions at room temperature is shown in Figure 2a and CL measurements in Figure 2b-d represent the SEM images of the typical single wires for the three samples with their corresponding CL hyperspectral signals. As the wire density is similar for the three samples, the direct comparison of PL intensity gives a rough indication of the luminescence efficiency. For all of them, we observe in Figure 2a the emissions of the InGaN QW around 440 nm and of the yellow-band (YB) defects centered at  $\sim 575 \text{ nm}$ .

A PL emission around 430 nm can be seen from sample #1 (direct SQW growth) in Figure 2a with the full width at half maximum (FWHM) of 280 meV. The sample #1 exhibits the lower

intensity with a possible wavelength variation from 420 to 460 nm. However, the CL mapping in Figure 2b shows almost no emission from the *m*-plane sidewalls. Measurements on different single wires confirm that the overall *m*-plane emission from SQW sample is negligible. Only the weak QW emission from the top facet can be observed for the present wire located around 2.8 eV (with a wire-to-wire variation down to 2.7 eV). Consequently, the PL emission observed for sample #1 is associated with QW located at the top facet and does not arise from the radial *m*-plane QW. The origin of light emission coming from the top facet can be attributed to *c*-plane facets or also semipolar facets present at the junction between *c*-plane and *m*-plane surfaces (see the supporting information).

For sample #2 and #3, the PL emission of the InGaN QW positioned around 435 nm (~2.85 eV) is observed in Figure 2a with the FWHM of 230 and 256 meV, respectively. For these two samples, the wavelength variation of QW emission peak is in the range of +/-10 nm. Another contribution occurs at 3.2 eV (~390 nm) only for the sample #3 evidencing the presence of InGaN UL with a low indium content estimated at ~5% from the PL emission.<sup>39</sup> Further, the related CL measurements for wire containing GaN spacer without and with InGaN UL (sample #2 and #3, respectively) clearly show an intense QW emission originating from the *m*-plane sidewalls (see Figure 2c,d) with intensity nearly two order in magnitude higher as compared to the *m*-plane QW emission from sample #1. This emission is located in the range of 2.7-2.9 eV, which is attributed to the indium fluctuations for a given target In composition.<sup>40</sup> We observe an overall slight redshift of the transition from the bottom to the top, as it is usually observed for such InGaN/GaN core-shell structures.<sup>41,42</sup> The detection of the top-facet emission for sample #2 and #3 is wire-to-wire dependent because of random morphology of top-facets related to possible

presence of residual Ga-polarity.<sup>43</sup> Such emission from top-facets is always weak in comparison of the *m*-plane emission. Also, Figure 2d shows the emission from InGaN UL localized around 3.2 eV all along the wire-sidewall without noticeable red-shift indicating much smaller indium fluctuations in agreement with the low-In content. This emission is present on full wire sidewalls and proves that the core-shell growth of low In-content InGaN UL is actually effective prior the QW growth on *m*-plane surfaces. The CL intensity between UL and SQW signals are changing in opposite way along the wire. On the SEM image, the wire becomes thicker along the direction of wire-top. Consequently, at the beginning of the core-shell region, more electron-hole pairs are generated in the GaN core and in the UL that enhances the emission of UL (carriers can then diffuse from the GaN core to the UL but cannot reach the QW). At the wire top, the increase of thickness limits the carrier generation into the GaN core and UL favoring the emission of SQW. In the same way, we notice that the acceleration voltage also plays a key role in the CL intensity of InGaN UL versus SQW, which is related to the excitation depth of e-beam (see the supporting information).

From these CL analyses, a direct comparison of PL intensities of sample #2 and #3 with sample #1 is not straightforward because the origin of SQW luminescence is different: either related to top facets for the sample #1 or related to *m*-facets for samples #2 and 3. We noticed that the emission from the sample #1 in both PL and CL emission exhibits one order of magnitude lower intensity compared to other two samples, whereas the similar intensity for both PL and CL measurements is observed for sample #2 and #3. The similar PL intensity of SQW with and w/o InGaN UL indicates the absence of efficiency improvement. This observation could point out that the thickness of UL chosen for the study may not be suitable for the core-shell structure. Therefore, a series of samples similar to sample #3 but with variable UL thickness (estimated

thickness varying from 50 to 200 nm) has been grown additionally and characterized by PL (see the supporting information). No significant improvement has been recorded in the QW emission as a function of the UL thickness. Finally, it is observed from the PL and CL measurements that the presence GaN spacer grown prior to the InGaN SQW allows the core-shell QW emission from *m*-plane facets.

Further investigation for the three samples is performed using temperature dependent PL experiment to study the competition between the radiative and non-radiative (NR) recombination as shown in Figure 3a-c. Assuming negligible NR recombination at low temperature, the luminescence intensity at room temperature is normalized with the intensity at low temperature to provide an estimation of the upper bound of the IQE.<sup>44,45</sup> The difference of the PL emission peak of the sample #1 compared to samples #2 and #3 at 5K is attributed to the different surface orientation of the SQW emission (top-facet vs *m*-plane facets). The emission of sample #1 comes from SQW on wire top-facet with possible polar or semipolar surface orientations, which can differently emit at low temperature combined maybe with screening effects for the polar *c*-plane QW. A low estimated IQE of 3.6% is measured for the sample #1 containing only top-facet SQW (see Figure 2b) indicating a high non-radiative recombination in such SQW. Concerning samples #2 and #3 containing GaN spacer - without and with UL (see Figure 3b,c), the IQE of *m*-plane SQW is estimated equal to 15.3% and 14.9% respectively. The presence of UL does not strongly change the IQE, pointing out the inefficiency of InGaN UL in the case of core-shell geometry, contrary to the usual planar *c*-plane QW structures. Moreover, a difference in the PL behavior (Figure 3b, 3c) is observed for the temperature around 150 K between sample #2 and #3, nevertheless if we consider the evolution of normalized intensity in Arrhenius plot (see supporting information) no significant change in activation energies is revealed. Also, in the

Figure 3c, the intensity decrease of UL when the PL temperature arises 300K is faster in comparison of SQW emission. This observation is explained by less carrier localizations due to a lower In-content of InGaN UL estimated around 5%.

Considering now that the results obtained in PL and in CL are not reliable techniques for comparing intensities of different samples (since it can be affected by the difference in extraction efficiency), we carried out a time-resolved CL (TRCL) analysis to estimate the light emission efficiency. In addition to the CL setup described above, a beam blanker has been used to generate short electron pulses and the recombination rate is measured using a fast photodetector. Details of the experimental setup can be found elsewhere.<sup>47</sup> Taking into account the size of the wires (about 1.5  $\mu\text{m}$  in diameter) and the rise time of the pulse generator, the temporal resolution is limited by the detector and estimated to be around 50 ps. The CL decay lifetime is calculated as follows in order to better understand and compare all samples. We first fit the experimental data with a mono-exponential decay:

$$I(t) = I_0 \exp\left(-\frac{t}{\tau}\right) \quad (1)$$

$$\frac{1}{\tau} = \frac{1}{\tau_r} + \frac{1}{\tau_{nr}} \quad (2)$$

where  $\tau$  is the effective lifetime considering both radiative ( $\tau_r$ ) and non-radiative ( $\tau_{nr}$ ) processes.

The internal quantum efficiency is then defined as  $\text{IQE} = \tau/\tau_r$ .

For each sample, we probe the ratio between the effective lifetime at room temperature compared to the one at low temperature. This allows us to compare the relative change of IQE between the

different samples. First, we perform the measurements at different temperatures on a single wire from sample #2 having GaN spacer as shown in Figure 4a. The decrease in effective lifetime with increasing temperature shown in Figure 4b is attributed to the activation of non-radiative processes – Shockley Read Hall (SRH) mechanism. We then study the influence of the UL by comparing the relative IQE of sample #2 (without UL) and sample #3 (with UL). To do so, we measure the effective lifetime for more than five wires for each sample at room temperature and also at 5K (see the inset of Figure 4b showing the ratio  $\tau_{\text{eff}}(300\text{K})/\tau_{\text{eff}}(5\text{K})$  for samples #2 and #3). No significant difference is recorded in the measured values at 5 or 300K. Also, the ratio remains in the 0.45-0.70 range (see averaged values indicated by dotted lines) indicating no large variation of effective lifetime, contrary to usual *c*-plane planar case, where the effective lifetime varies by two orders of magnitude (from 170 ps to 20 ns) by adding an InGaN UL.<sup>33</sup>

TRPL has been performed at room temperature on wire ensemble in order to deduce the average effective lifetime for a large number of wires. The as-grown wires are dispersed on silicon substrates and excited with 366 nm laser operating with a power density of 1.73 W/cm<sup>2</sup> and having a repetition rate of 76.0 MHz. Figure 4c corresponds to the PL decay measured for sample #2 (without UL) and sample #3 (with UL) respectively. The estimated effective carrier lifetimes ( $\tau_{\text{eff}}$ ) for the two samples show no significant difference (133 ps and 145 ps for sample #2 and sample #3 respectively), thus being consistent with the TRCL measurements. Therefore, the overall optical measurements do not show any IQE improvement by adding an UL to the *m*-plane QW.

**Structural Characterizations.** To further understand the influence of the GaN spacer on the growth of the InGaN QW and to correlate the growth results to the improved light emission, two additional typical core-shell InGaN samples without and with GaN spacer are studied by STEM.

Note that unlike the samples characterized above which contain single QW, additional samples studied by STEM have MQWs so as to observe the propagation of structural defects (if any). The samples studied by STEM correspond to typical core-shell MQWs grown at 750°C for InGaN QWs and at 885°C for the GaN barriers. The same process explained for the SQW growth is performed on these core-shell MQW systems. Thin cross-section slices of the wires either in longitudinal or in transversal mode (cutting along and perpendicular to the  $c$ -axis, respectively) are prepared by focused ion beam (FIB) using a STRATA 400S equipment. First STEM analyses (see Figures 5a,c) at low magnification are performed on a FEI TECNAI microscope operated at 200 kV using a High Angle Annular Dark Field detector (HAADF) with a rather large camera length to enhance the diffraction contrast related to the presence of defects with respect to the chemical contrast. The core-shell InGaN QWs in these STEM images appear bright and the GaN barriers look dark. Figure 5a reveals a significant number of bright lines corresponding to extended defects originating from the first QW when the QWs are directly grown on wire sidewalls, whereas no defect is visible in the case of GaN spacer growth (Figure 5c). The Figure S6 in the supporting information shows a STEM image of selected zone with and w/o GaN spacer that clearly confirms the absence of extended defects in presence of the GaN spacer. InGaN/GaN core-shell wires usually exhibit stacking faults (SFs) showing contrast perpendicular to the QWs.<sup>4,48</sup> Detailed investigation of the SFs in the case of planar QWs on  $m$ -plane GaN systems reveals that these defects plastically relax the misfit strain accumulated during the growth process along the  $\bar{c}$ -direction.<sup>49,50</sup> The pronounced difference between the defect densities in the two images is clearly related to the growth of the GaN spacer. It demonstrates that the presence of GaN spacer grown at lower temperature prevents the formation of extended defects which cause the degradation of the QWs properties. To understand the origin of defect formation, STEM-HAADF images at high magnification combined with energy dispersive X-ray (EDX)

spectra are acquired using a FEI THEMIS operated at 200 kV and equipped with super X detectors. Figure 5b,d shows the STEM images and EDX mapping including Si (yellow), In (red) and Ga (green) elements for the two samples having InGaN/GaN QWs without and with GaN spacer, respectively. In Figure 5d, the presence of a GaN spacer having a thickness of ~150 nm is clearly visible separating the GaN core from the first QW as indicated by a narrow dark line pointed by two yellow arrows. EDX mapping reveals the presence of Si inside this dark line. Therefore, an ultra-thin Si-enriched layer corresponding probably to  $\text{SiGa}_x\text{N}_y$  seems to be spontaneously formed on GaN wire sidewalls when the wire growth is stopped to reach the MQW growth conditions. In the high-resolution STEM image (image at left side in Figure 5d), the thickness of this residual layer is about 1 nm. Ultra-thin layer in core-shell MQW wires has also been previously reported<sup>51,52,53</sup> and related to Si-enrichment as shown by EDX measurements.<sup>6,54,55</sup> This contaminated layer formation is attributed to some residual silane that may be still present in the reactor, because of the high flux silane injection used to passivate the lateral surface<sup>56</sup> around the wire-stem during the first stage of the GaN wire growth. When the silane flux is stopped, ‘a memory effect’ can lead to an unintentional thin  $\text{SiGa}_x\text{N}_y$  deposition and eventually to a Si surface segregation. We can notice that this surface contamination adversely affects the growth of the first InGaN QW as can be seen in Figure 5b. Indeed, the EDX mapping (bottom image) highlights the presence of an ultra-thin layer containing Si at the interface between the GaN wire sidewalls and the first InGaN QW. The presence of this unintentionally formed layer having a thickness of about 1 nm (as revealed by HR-STEM image on the left side of Figure 5b) is detrimental for the first QW grown immediately after the GaN core, exhibiting rough interfaces, a large thickness gradient and the nucleation of a high-density of extended defects. The  $\text{SiN}_x$  layer is known to act as a passivation layer in selective area growth and prevents growth of (In)GaN. Therefore, we can suspect that this residual  $\text{SiGa}_x\text{N}_y$  layer highly

perturbs the InGaN QW growth. In Figure 5a, a small hole is even visible (see the black circle) on the first QW related to an effect of selective area growth of InGaN on the  $\text{SiGa}_x\text{N}_y$  layer. The presence of such holes has been already observed in some of our previous works.<sup>4,57</sup> The actual growth of (In)GaN on this residual  $\text{SiGa}_x\text{N}_y$  ultra-thin layer is certainly related to the discontinuity and non-stoichiometry of this unintended layer. The fact that no defect is generated at the SiGaN/GaN interface (contrary to the SiGaN/InGaN interface) is consistent with the growth of high quality GaN on *in situ*  $\text{SiN}_x$  intermediate layer acting as a dislocation filtering previously reported for planar growth.<sup>58</sup> The defects induced by the  $\text{SiGa}_x\text{N}_y$  layer on InGaN favor the non-radiative recombination and degrades the light emission efficiency. The growth of GaN spacer allows burying this unintentional  $\text{SiGa}_x\text{N}_y$  layer in order to prevent the defect formation inside InGaN MQW stacks. This observation is consistent with the previous optical characterization confirming that GaN spacer growth is required to get m-plane emission and to provide performance improvement.<sup>59</sup>

Apart from the beneficial role of GaN spacer, another important finding from our experimental results is that the introduction of an InGaN UL does not improve the IQE of the core-shell active region in stark contrast to *c*-plane QWs.<sup>33</sup> Such a drastic change when moving from *c*-plane QW to *m*-plane QW, might be linked to the strong increase of residual doping observed in *m*-plane QWs compared to *c*-plane QW which may lead to an apparent increase of IQE.<sup>60</sup> However, similar experiments have been performed on n-GaN core/active region/p-GaN shell, in order to place the active region in the center of the space charge region to reduce the effect of the residual doping. These experiments (data not shown) lead to similar conclusions, *i.e.* the UL does not improve *m*-plane QW IQE. One may wonder if the surface point defect density is lower in our sample due to the intrinsic role of the *m*-plane surface or to our growth conditions having a very

low V/III ratio. It has been shown on *c*-plane QWs that point surface defects are created only when the GaN buffer is grown at high temperature ( $> 850^{\circ}\text{C}$ ) associated with a thermal activation energy of 3.6 eV close to the decomposition activation of *c*-plane GaN.<sup>33</sup> In addition, it has been observed that the deep level density is drastically reduced for N-type *m*-plane GaN compared to the *c*-plane GaN.<sup>61</sup> Therefore, the inefficiency of InGaN UL on *m*-plane wire facets is certainly attributed to the reduction of point defect density related either to an intrinsic property of *m*-plane GaN surfaces or to an extrinsic property due to unusual growth conditions required to form wires.

## CONCLUSIONS

In conclusion, a detailed analysis correlating optical and structural characterization has been performed on Si-doped  $\bar{c}$ -wires with *m*-plane core-shell InGaN/GaN QWs to study the influence of GaN spacer and low In-content InGaN UL on the InGaN SQW emission efficiency. The PL and CL measurements reveal that for the sample with direct growth of SQW, no *m*-plane emission is measured whereas this emission is observed for sample having GaN spacer (with and without InGaN UL) exhibiting an IQE of about 15%. No significant change of  $\tau_{\text{eff}}$  is measured in presence of InGaN UL by TR-CL at 5 and 300K or by TR-PL at 300K proving that no IQE improvement is effective for core-shell *m*-plane QW. The *m*-plane emission of SQW is explained by the structural observations obtained by STEM since the presence of 150 nm-thick GaN spacer prevents the degradation of InGaN QWs induced by an unintended ultra-thin  $\text{SiGa}_x\text{N}_y$  layer present around the GaN core. The growth of GaN spacer results in well-defined QWs without the formation of any extended defects. On the contrary, the presence of low In-content InGaN UL does not further improve the SQW efficiency, whereas such UL has been proposed to explain the strong enhancement of the emission efficiency for standard planar *c*-InGaN/GaN MQWs. If we

assume the explanations proposed for the 2D materials ruling out the importance of extended defects for QW emission efficiency, the density of point defects in these wires would be considered less significant to act as NR centers and a single GaN spacer is definitely sufficient to prevent the QW efficiency degradation. The surface formation energy of the point defects such as vacancy is certainly different for *c*-plane GaN to *m*-plane GaN. Additional *ab-initio* calculations and growth experiments on planar *m*-plane LED containing UL are required to extend this effect on all types of *m*-plane surfaces.

## **ACKNOWLEDGMENTS**

This work has been financially supported by French National Labex GaNeX (ANR-11-LABX-2014). The authors would like to thank J. Dussaud for his work on the MOVPE setup and N. Mollard for his support in FIB preparation. The authors would also like to acknowledge D. Salomon, A. Dussaigne, P. Ferret, P. Gilet for preliminary work on GaN spacers and N. Grandjean for fruitful discussions on InGaN UL.

## **ASSOCIATED CONTENT**

### **Supporting Information**

Photoluminescence measurement for as-grown wires on sapphire substrate having varying thickness of UL (between 50-200 nm), cathodoluminescence (CL) measurement for sample #3 as a function of accelerating voltage (0.5-30 kV), additional hyperspectral CL analyses for single wires from sample #1, time-resolved CL measurements for single wire from sample #2, STEM

image showing absence and presence of extended defects in the same wire slice, Arrhenius plot for sample #2 and #3 to understand the different PL evolution at varying temperatures.

### **Figure Caption**

**Figure 1:** Schematics of the three core-shell heterostructures grown on  $\bar{c}$ -oriented GaN wires: (a) #1 InGaN single quantum well (SQW), (b) #2 with the addition of a GaN spacer prior to SQW, (c) #3 with the adding of an InGaN under-layer (UL) between the GaN spacer and the SQW. 30°-tilted SEM images of as-grown wires: (d), (e) and (f) corresponds to (a), (b) and (c) heterostructures respectively along with enlarged views on single wires.

**Figure 2:** Optical measurements at room temperature: (a) PL spectra for the three as-grown samples presented in Figure 1, (b)-(d) CL hyperspectral analysis of typical single wires with the SEM image view of the measured wires for three samples.

**Figure 3:** Temperature dependent PL spectra for the three as-grown samples: #1 SQW (a), #2 GaN spacer addition prior SQW (b) and #3 InGaN under-layer (UL) between the GaN spacer and the SQW (c). Internal quantum efficiency (IQE) estimation is provided for samples #2 and #3 related to  $m$ -plane emission (the sample #1 exhibits emission from top-facets).

**Figure 4:** Time resolved measurements using TRCL (a,b) and TRPL (c): (a) TRCL intensity decay curves as a function of temperature for the sample #2, (b) effective lifetime ( $\tau_{\text{eff}}$ ) at 5 and 300K measured on 5 different wires coming from sample #2 and #3 (effective lifetime as a function of temperature measured on one wire of sample #2), the inset compares the ratio  $\tau_{\text{eff}}(300\text{K})/\tau_{\text{eff}}(5\text{K})$  for wires of the sample #2 (without UL) and the sample #3 (with UL); (c) TRPL intensity decay curves for sample #2 and #3 showing estimated values for  $\tau_{300\text{K}}$  as 132 and 145 ps respectively.

**Figure 5:** STEM-HAADF images at low (a,c) and high magnification (b,d) for samples with (a,b) and without (c,d) GaN spacer (150 nm thick) of core-shell InGaN/GaN MQW systems. EDX maps complete the high magnification observation. (a,b): Transversal cross-sectional STEM-HAADF images taken along the [0001] zone axis. The enlarged image (left image in (b)) corresponding to the blue square of the right image shows the presence of a dark line at the interface between the GaN core (yellow arrow) and the first QW, STEM-EDX elemental map of Ga (green), In (red) and Si (yellow) (bottom image in (b)) indicates that the dark line is a Si-enriched layer; (c,d) Longitudinal cross-sectional STEM-HAADF images taken along the  $[10\bar{1}0]$  zone axis. The enlarged image (left image in (d)) and STEM-EDX elemental map (bottom image in (d)) show that the Si-enriched layer (dark line) is located at the interface between the GaN core and the GaN spacer, far away from the first InGaN QW.

## Bibliography

- (1) Damilano, B.; Gil, B. Yellow-Red Emission from (Ga,In)N Heterostructures. *J. Phys. D. Appl. Phys.* **2015**, *48*, 403001.
- (2) Narukawa, Y.; Ichikawa, M.; Sanga, D.; Sano, M.; Mukai, T. White Light Emitting Diodes with Super-High Luminous Efficacy. *J. Phys. D. Appl. Phys.* **2010**, *43*, 354002.
- (3) Takeuchi, T.; Sota, S.; Katsuragawa, M.; Komori, M.; Takeuchi, H.; Amano, H.; Akasaki, I. Quantum-Confined Stark Effect Due to Piezoelectric Fields in GaInN Strained Quantum Wells. *Jpn. J. Appl. Phys.* **1997**, *36*, L382–L385.
- (4) Koester, R.; Hwang, J.; Salomon, D.; Chen, X.; Bougerol, C.; Barnes, J.; Le Si Dang, D.; Rigutti, L.; Bugallo, A. D. L.; Jacopin, G.; Tchernycheva, M.; Durand, C.; Eymery, J. M-Plane Core-Shell InGaN/GaN Multiple-Quantum-Wells on GaN Wires for Electroluminescent Devices. *Nano Lett.* **2011**, *11*, 4839–4845.
- (5) Li, S.; Waag, A. GaN Based Nanorods for Solid State Lighting. *J. Appl. Phys.* **2012**, *111*, 071101.
- (6) Tessarek, C.; Heilmann, M.; Butzen, E.; Haab, A.; Hardtdegen, H.; Dieker, C.; Spiecker, E.; Christiansen, S. The Role of Si during the Growth of Gan Micro- and Nanorods. *Cryst. Growth Des.* **2014**, *14*, 1486–1492.

- (7) Ra, Y. H.; Navamathavan, R.; Kang, S.; Lee, C. R. Different Characteristics of InGaN/GaN Multiple Quantum Well Heterostructures Grown on m- and r-Planes of a Single n-GaN Nanowire Using Metalorganic Chemical Vapor Deposition. *J. Mater. Chem. C* **2014**, *2*, 2692–2701.
- (8) Schimpke, T.; Martin, M.; Stoll, I.; Pohl-Klein, B.; Bichler, D.; Franz, Z.; Strube-knyrim, J.; Huckenbeck, B.; Max, B.; Marcus, M.; Veit, P.; Bertram, F.; Christen, J.; Hartmann, J.; Waag, A.; Lugauer, H.; Strassburg, M. Phosphor-Converted White Light from Blue-Emitting InGaN Microrod LEDs. *Phys. stat. sol.* **2016**, *213* (6), 1577–1584.
- (9) Qian, F.; Li, Y.; Gradecak, S.; Park, H.; Dong, Y.; Ding, Y.; Wang, Z. L.; Lieber, C. M. Multi-Quantum-Well Nanowire Heterostructures for Wavelength-Controlled Lasers. *Nat. Mater.* **2008**, *7*, 701–706.
- (10) Salomon, D.; Dussaigne, A.; Lafossas, M.; Durand, C.; Bougerol, C.; Ferret, P.; Eymery, J. Metal Organic Vapour-Phase Epitaxy Growth of GaN Wires on Si (111) for Light-Emitting Diode Applications. *Nanoscale Res. Lett.* **2013**, *8* (61), 1–5.
- (11) Koester, R.; Hwang, J. S.; Durand, C.; Dang, D. L. S.; Eymery, J. Self-Assembled Growth of Catalyst-Free GaN Wires by Metal-Organic Vapour Phase Epitaxy. *Nanotechnology* **2010**, *21*, 015602.
- (12) Coulon, P. M.; Mexis, M.; Teisseire, M.; Jublot, M.; Vennéguès, P.; Leroux, M.; Zuniga-Perez, J. Dual-Polarity GaN Micropillars Grown by Metalorganic Vapour Phase Epitaxy : Cross- Correlation between Structural and Optical Properties. *J. Appl. Phys.* **2014**, *115*, 153504.
- (13) Hersee, S. D.; Rishinaramangalam, A. K.; Fairchild, M. N. Threading Defect Elimination

in GaN Nanowires. *J. Mater. Res.* **2011**, *26* (17), 2293–2298.

- (14) Tu, C.-G.; Liao, C.-H.; Yao, Y.-F.; Chen, H.-S.; Lin, C.-H.; Su, C.-Y.; Shih, P.-Y.; Chen, W.-H.; Zhu, E.; Kiang, Y.-W.; Yang, C. C. Regularly Patterned Non-Polar InGaN/GaN Quantum-Well Nanorod Light-Emitting Diode Array. *Opt. Express* **2014**, *22* (S7), A1799.
- (15) Guan, N.; Dai, X.; Messanvi, A.; Zhang, H.; Yan, J.; Gautier, E.; Bougerol, C.; Julien, F. H.; Durand, C.; Eymery, J.; Tchernycheva, M. Flexible White Light Emitting Diodes Based on Nitride Nanowires and Nanophosphors. *ACS Photonics* **2016**, *3*, 597–603.
- (16) Dai, X.; Messanvi, A.; Zhang, H.; Durand, C.; Eymery, J.; Bougerol, C.; Julien, F. H.; Tchernycheva, M. Flexible Light-Emitting Diodes Based on Vertical Nitride Nanowires. *Nano Lett.* **2015**, *15*, 6958–6964.
- (17) Zhang, H.; Dai, X.; Guan, N.; Messanvi, A.; Neplokh, V.; Piazza, V.; Vallo, M.; Bougerol, C.; Julien, F. H.; Babichev, A.; Cavassilas, N.; Bescond, M.; Michelini, F.; Foldyna, M.; Gautier, E.; Durand, C.; Eymery, J.; Tchernycheva, M. Flexible Photodiodes Based on Nitride Core/Shell p – n Junction Nanowires. *ACS Appl. Mater. Interfaces* **2016**, *8*, 26198–26206.
- (18) Chung, K.; Beak, H.; Tchoe, Y.; Oh, H.; Yoo, H.; Kim, M.; Yi, G. C. Growth and Characterizations of GaN Micro-Rods on Graphene Films for Flexible Light Emitting Diodes. *APL Mater.* **2014**, *2*, 092512.
- (19) Nami, M.; Rashidi, A.; Monavarian, M.; Mishkat-Ul-Masabih, S.; Rishinaramangalam, A. K.; Brueck, S. R. J.; Feezell, D. Electrically Injected GHz-Class GaN/InGaN Core-Shell Nanowire-Based MLEDs: Carrier Dynamics and Nanoscale Homogeneity. *ACS Photonics* **2019**, *6*, 1618–1625.

- (20) Mohajerani, M. S.; Marcus, M.; Hartmann, J.; Zhou, H.; Wehmann, H. H.; Veit, P.; Bertam, F.; Christen, J.; Waag, A. Direct Correlations of Structural and Optical Properties of Three-Dimensional GaN / InGaN Core / Shell Micro-Light Emitting Diodes. *Jpn. J. Appl. Phys.* **2016**, *55*, 05FJ09.
- (21) Lu, W.; Sone, N.; Goto, N.; Iida, K.; Suzuki, A.; Han, D. P.; Iwaya, M.; Tekeuchi, T.; Kamiyama, S.; Akasaki, I. Effect of AlGaN Undershell on the Cathodoluminescence Properties of Coaxial GaInN/GaN Multiple-Quantum-Shells Nanowires. *Nanoscale* **2019**, *11*, 18746–18757.
- (22) Lu, W.; Terazawa, M.; Han, D.; Sone, N.; Goto, N.; Iida, K.; Murakami, H.; Iwaya, M.; Tekeuchi, T.; Kamiyama, S.; Isamu, A. Structural and Optical Impacts of AlGaN Undershells on Coaxial GaInN / GaN Multiple-Quantum-Shells Nanowires. *Nanophotonics* **2019**.
- (23) Rishinaramangalam, A. K.; Nami, M.; Shima, D. M.; Balakrishnan, G.; Brueck, S. R. J.; Feezell, D. F. Reduction of Reverse-Leakage Current in Selective-Area-Grown GaN-Based Core–Shell Nanostructure LEDs Using AlGaN Layers. *Phys. Status Solidi* **2017**, *214* (5), 1600776.
- (24) Nami, M.; Stricklin, I. E.; Davico, K. M.; Mishkat-ul-masabih, S.; Rishinaramangalam, A. K.; Brueck, S. R. J.; Brener, I.; Feezell, D. F. Carrier Dynamics and Electro- Optical Characterization of High- Performance GaN / InGaN Core-Shell Nanowire Light-Emitting Diodes. *Sci. Rep.* **2018**, *8* (501), 1–11.
- (25) Schimpke, T.; Lugauer, H.-J.; Avramescu, A.; Varghese, T.; Koller, A.; Hartmann, J.; Ledig, J.; Waag, A.; Strassburg, M. Position-Controlled MOVPE Growth and Electro-

Optical Characterization of Core-Shell InGaN/GaN Microrod LEDs. *Proc. SPIE* **2016**, 9768, 97680T.

- (26) Sugimoto, K.; Denpo, Y.; Okada, N.; Tadatomo, K. Effect of Superlattice on Light Output Power of InGaN-Based Light-Emitting Diodes Fabricated on Underlying GaN Substrates with Different Dislocation Densities. *Phys. Status Solidi* **2016**, 13 (5–6), 270–273.
- (27) Mu, Q.; Xu, M.; Wang, X.; Wang, Q.; Lv, Y.; Feng, Z.; Xu, X.; Ji, Z. Influence of the InGaN/GaN Quasi-Superlattice Underlying Layer on Photoluminescence in InGaN/GaN Multiple Quantum Wells. *Phys. E* **2016**, 76, 1–5.
- (28) Davies, M. J.; Dawson, P.; Massabuau, F. C. P.; Fol, A. Le; Oliver, R. A.; Kappers, M. J.; Humphreys, C. J. A Study of the Inclusion of Prelayers in InGaN/GaN Single- and Multiple-Quantum-Well Structures. *Phys. Status Solidi* **2015**, 252 (5), 866–872.
- (29) Akasaka, T.; Gotoh, H.; Saito, T.; Makimoto, T. High Luminescent Efficiency of InGaN Multiple Quantum Wells Grown on InGaN Underlying Layers. *Appl. Phys. Lett.* **2004**, 85, 3089–3091.
- (30) Otsuji, N.; Fujiwara, K.; Sheu, J. K. Electroluminescence Efficiency of Blue InGaN/GaN Quantum-Well Diodes with and without an n-InGaN Electron Reservoir Layer. *J. Appl. Phys.* **2006**, 100, 113105.
- (31) Armstrong, A. M.; Bryant, B. N.; Crawford, M. H.; Koleske, D. D.; Lee, S. R.; Wierer, J. J. Defect-Reduction Mechanism for Improving Radiative Efficiency in InGaN/GaN Light-Emitting Diodes Using InGaN Underlayers. *J. Appl. Phys.* **2015**, 117, 134501.
- (32) Haller, C.; Carlin, J. F.; Jacopin, G.; Martin, D.; Butté, R.; Grandjean, N. Burying Non-Radiative Defects in InGaN Underlayer to Increase InGaN/GaN Quantum Well Efficiency.

*Appl. Phys. Lett.* **2017**, *111*, 262101.

- (33) Haller, C.; Carlin, J.-F.; Jacopin, G.; Liu, W.; Martin, D.; Butté, R.; Grandjean, N. GaN Surface as the Source of Non-Radiative Defects in InGaN/GaN Quantum Wells. *Appl. Phys. Lett.* **2018**, *113*, 111106.
- (34) Dominec, F.; Hospodková, A.; Hubáček, T.; Zíková, M.; Pangrác, J.; Kuldová, K.; Vetushka, A.; Hulicius, E. Influence of GaN Buffer Layer under InGaN/GaN MQWs on Luminescent Properties. *J. Cryst. Growth* **2019**, *507*, 246–250.
- (35) Tchoufian, P.; Donatini, F.; Levy, F.; Amstatt, B.; Ferret, P.; Pernot, J. High Conductivity in Si-Doped GaN Wires. *Appl. Phys. Lett.* **2013**, *102*, 122116.
- (36) Tchoufian, P.; Donatini, F.; Levy, F.; Amstatt, B.; Dussaigne, A.; Ferret, P.; Bustarret, E.; Pernot, J. Thermoelectric and Micro-Raman Measurements of Carrier Density and Mobility in Heavily Si-Doped GaN Wires. *Appl. Phys. Lett.* **2013**, *103*, 202101.
- (37) Tchoufian, P.; Donatini, F.; Levy, F.; Dussaigne, A.; Ferret, P.; Pernot, J. Direct Imaging of P-n Junction in Core-Shell GaN Wires. *Nano Lett.* **2014**, *14*, 3491–3498.
- (38) Eymery, J.; Salomon, D.; Chen, X.; Durand, C. Process for Catalyst-Free Selective Growth on a Semiconductor Structure. *Pat. WO/2012/136665*, Oct. 11, **2012**.
- (39) Pelá, R. R.; Caetano, C.; Marques, M.; Ferreira, L. G.; Furthmüller, J.; Teles, L. K. Accurate Band Gaps of AlGa<sub>N</sub>, InGa<sub>N</sub>, and AlInN Alloys Calculations Based on LDA-1/2 Approach. *Appl. Phys. Lett.* **2011**, *98*, 151907.
- (40) Auf Der Maur, M.; Pecchia, A.; Penazzi, G.; Rodrigues, W.; Di Carlo, A. Efficiency Drop in Green InGa<sub>N</sub>/Ga<sub>N</sub> Light Emitting Diodes: The Role of Random Alloy Fluctuations.

*Phys. Rev. Lett.* **2016**, *116*, 027401.

- (41) Shahmohammadi, M.; Ganière, J. D.; Zhang, H.; Ciechonski, R.; Vescovi, G.; Kryliouk, O.; Tchernycheva, M.; Jacopin, G. Excitonic Diffusion in InGaN/GaN Core-Shell Nanowires. *Nano Lett.* **2016**, *16*, 243–249.
- (42) Liu, W.; Mounir, C.; Rossbach, G.; Schimpke, T.; Avramescu, A.; Lugauer, H. J.; Strassburg, M.; Schwarz, U.; Deveaud, B.; Jacopin, G. Spatially Dependent Carrier Dynamics in Single InGaN/GaN Core-Shell Microrod by Time-Resolved Cathodoluminescence. *Appl. Phys. Lett.* **2018**, *112*, 052106.
- (43) Chen, X. J.; Perillat-Merceroz, G.; Sam-Giao, D.; Durand, C.; Eymery, J. Homoepitaxial Growth of Catalyst-Free GaN Wires on N-Polar Substrates. *Appl. Phys. Lett.* **2010**, *97*, 151909.
- (44) Murotani, H.; Yamada, Y.; Tabata, T.; Honda, Y.; Yamaguchi, M.; Amano, H. Effects of Exciton Localization on Internal Quantum Efficiency of InGaN Nanowires. *J. Appl. Phys.* **2013**, *114*, 153506.
- (45) Watanabe, S.; Yamada, N.; Nagashima, M.; Ueki, Y.; Sasaki, C.; Yamada, Y.; Taguchi, T.; Tadatomo, K.; Okagawa, H.; Kudo, H. Internal Quantum Efficiency of Highly-Efficient In<sub>x</sub>Ga<sub>1-x</sub>N-Based near-Ultraviolet Light-Emitting Diodes. *Appl. Phys. Lett.* **2003**, *83*, 4906–4908.
- (46) Le Boulbar, E. D.; Edwards, P. R.; Vajargah, S. H.; Griffiths, I.; Gîrgel, I.; Coulon, P. M.; Cherns, D.; Martin, R. W.; Humphreys, C. J.; Bowen, C. R.; Allsopp, D.- W.E.; Shields, P.- A. Structural and Optical Emission Uniformity of M-Plane InGaN Single Quantum Wells in Core-Shell Nanorods. *Cryst. Growth Des.* **2016**, *16*, 1907–1916.

- (47) Donatini, F.; Pernot, J. Exciton Diffusion Coefficient Measurement in ZnO Nanowires under Electron Beam Irradiation. *Nanotechnology* **2018**, *29*, 105703.
- (48) Mancini, L.; Hernández-Maldonado, D.; Lefebvre, W.; Houard, J.; Blum, I.; Vurpillot, F.; Eymery, J.; Durand, C.; Tchernycheva, M.; Rigutti, L. Multi-Microscopy Study of the Influence of Stacking Faults and Three-Dimensional In Distribution on the Optical Properties of m-Plane InGaN Quantum Wells Grown on Microwire Sidewalls. *Appl. Phys. Lett.* **2016**, *108*, 042102.
- (49) Fischer, A. M.; Wu, Z.; Sun, K.; Wei, Q.; Huang, Y.; Senda, R.; Iida, D.; Iwaya, M.; Amano, H.; Ponce, F. A. Misfit Strain Relaxation by Stacking Fault Generation in InGaN Quantum Wells Grown on M-Plane GaN. *Appl. Phys. Express* **2009**, *2*, 041002.
- (50) Krause, T.; Hanke, M.; Nicolai, L.; Cheng, Z.; Niehle, M.; Trampert, A. Structure and Composition of Isolated Core-Shell (In,Ga) N/GaN Rods Based on Nanofocus X-Ray Diffraction and Scanning Transmission Electron Microscopy. *Phys. Rev. Appl.* **2017**, *7*, 024033.
- (51) Mandl, M.; Wang, X.; Schimpke, T.; Kölper, C.; Binder, M.; Ledig, J.; Waag, A.; Kong, X.; Trampert, A.; Bertram, F.; Christen, J.; Barbagini, F.; Calleja, E.; Strassburg, M. Group III Nitride Core-Shell Nano- and Microrods for Optoelectronic Applications. *Phys. Status Solidi - Rapid Res. Lett.* **2013**, *7* (10), 800–814.
- (52) Yi, W.; Uzuhashi, J.; Chen, J.; Kimura, T.; Kamiyama, S.; Takeuchi, T.; Ohkubo, T.; Sekiguchi, T.; Hono, K. Cathodoluminescence and Scanning Transmission Electron Microscopy Study of InGaN/GaN Quantum Wells in Core-Shell GaN Nanowires. *Appl. Phys. Express* **2019**, *12*, 085003.

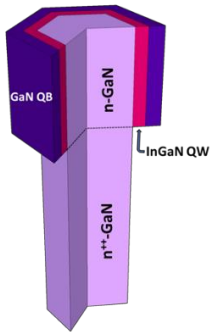
- (53) Durand, C.; Bougerol, C.; Carlin, J. F.; Rossbach, G.; Godel, F.; Eymery, J.; Jouneau, P. H.; Mukhtarova, A.; Butté, R.; Grandjean, N. M-Plane GaN/InAlN Multiple Quantum Wells in Core-Shell Wire Structure for UV Emission. *ACS Photonics* **2014**, *1*, 38–46.
- (54) Ren, C. X.; Tang, F.; Oliver, R. A.; Zhu, T. Nanoscopic Insights into the Effect of Silicon on Core-Shell InGaN/GaN Nanorods: Luminescence, Composition, and Structure. *J. Appl. Phys.* **2018**, *123*, 045103.
- (55) Tessarek, C.; Rechberger, S.; Dieker, C.; Heilmann, M.; Spiecker, E.; Christiansen, S. Understanding GaN/InGaN Core-Shell Growth towards High Quality Factor Whispering Gallery Modes from Non-Polar InGaN Quantum Wells on GaN Rods. *Nanotechnology* **2017**, *28*, 485601.
- (56) Markurt, T.; Lymperakis, L.; Neugebauer, J.; Drechsel, P.; Stauss, P.; Schulz, T.; Remmele, T.; Grillo, V.; Rotunno, E.; Albrecht, M. Blocking Growth by an Electrically Active Subsurface Layer: The Effect of Si as an Antisurfactant in the Growth of GaN. *Phys. Rev. Lett.* **2013**, *110*, 036103.
- (57) Messanvi, A.; Zhang, H.; Neplokh, V.; Julien, F. H.; Bayle, F.; Foldyna, M.; Bougerol, C.; Gautier, E.; Babichev, A.; Durand, C.; Eymery, J. Tchernycheva, M. Investigation of Photovoltaic Properties of Single Core-Shell GaN/InGaN Wires. *ACS Appl. Mater. Interfaces* **2015**, *7*, 21898–21906.
- (58) Kappers, M. J.; Datta, R.; Oliver, R. A.; Rayment, F. D. G.; Vickers, M. E.; Humphreys, C. J. Threading Dislocation Reduction in (0 0 01) GaN Thin Films Using SiN<sub>x</sub> Interlayers. *J. Cryst. Growth* **2007**, *300*, 70–74.
- (59) Gilet, P.; Dussaigne, A.; Salomon, D.; Eymery, J.; Durand, C. Optoelectronic Device

Comprising Three-Dimensional Semiconductors Elements, and Method for Manufacturing Said Device. *US Pat. App. 15/745,429, July 26, 2018*.

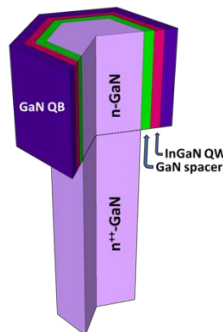
- (60) Liu, W.; Butté, R.; Dussaigne, A.; Grandjean, N.; Deveaud, B.; Jacopin, G. Carrier-Density-Dependent Recombination Dynamics of Excitons and Electron-Hole Plasma in m-Plane InGaN/GaN Quantum Wells. *Phys. Rev. B* **2016**, *94*, 195411.
- (61) Henry, T. A.; Armstrong, A.; Kelchner, K. M.; Nakamura, S.; Denbaars, S. P.; Speck, J. S. Assessment of Deep Level Defects in M-Plane GaN Grown by Metalorganic Chemical Vapor Deposition. *Appl. Phys. Lett.* **2012**, *100*, 082103.

Figure 1

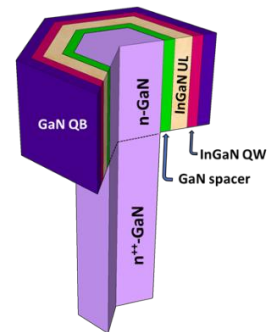
(a) #1: SQW



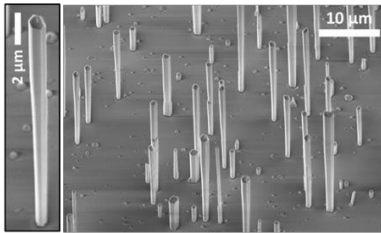
(b) #2: GaN spacer + SQW



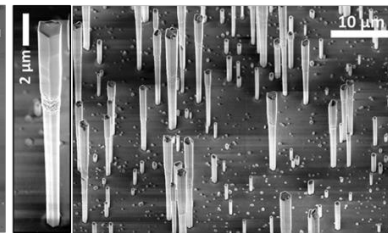
(c) #3: GaN spacer + UL + SQW



(d)



(e)



(f)

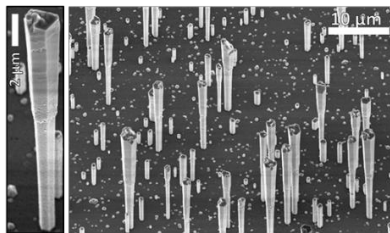


Figure 2

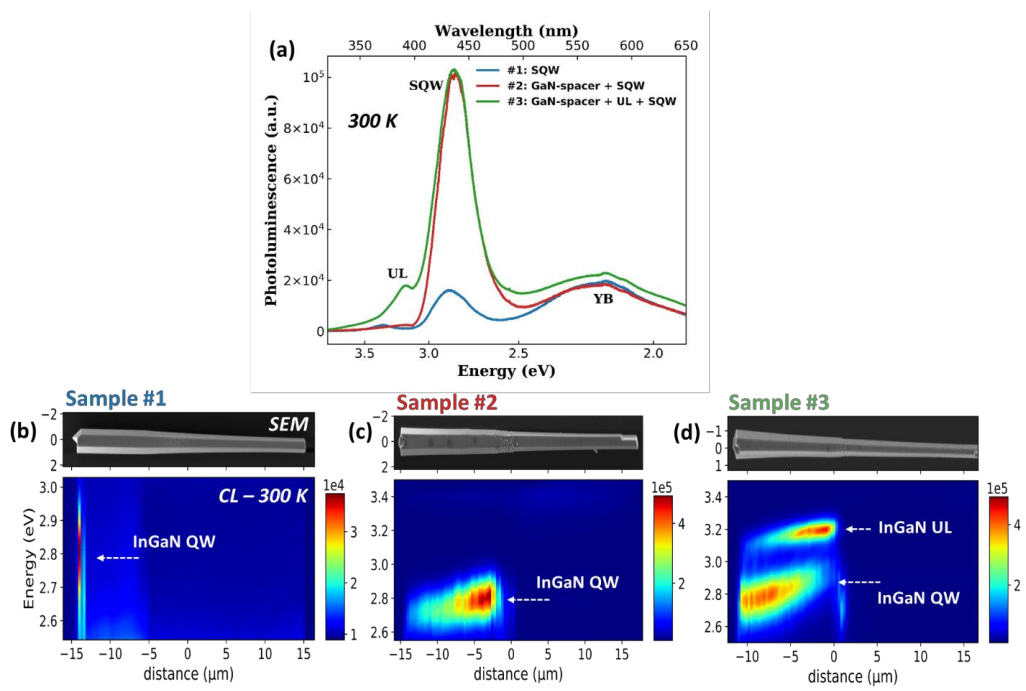


Figure 3

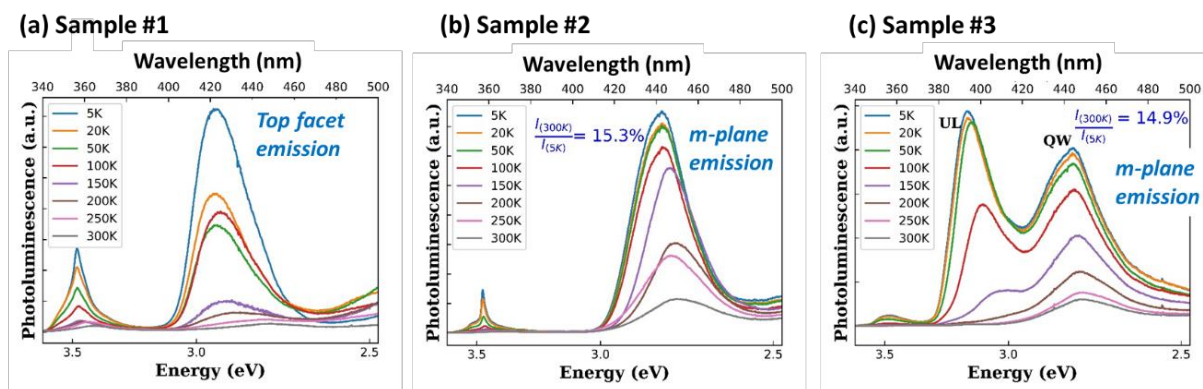


Figure 4

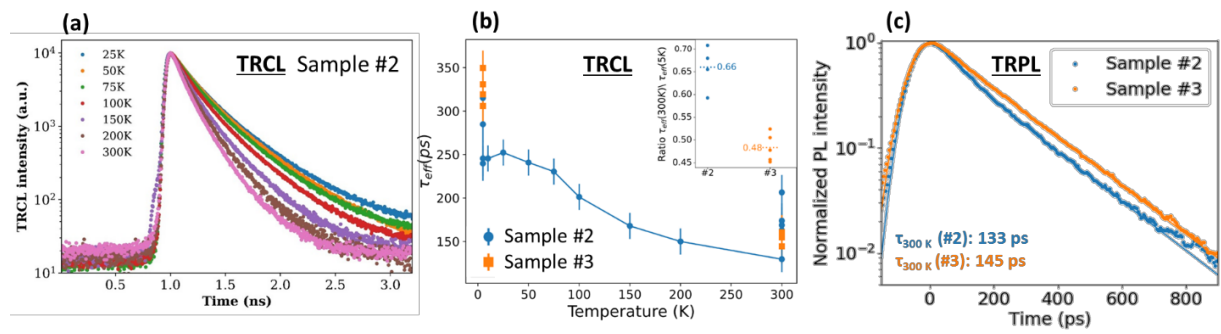
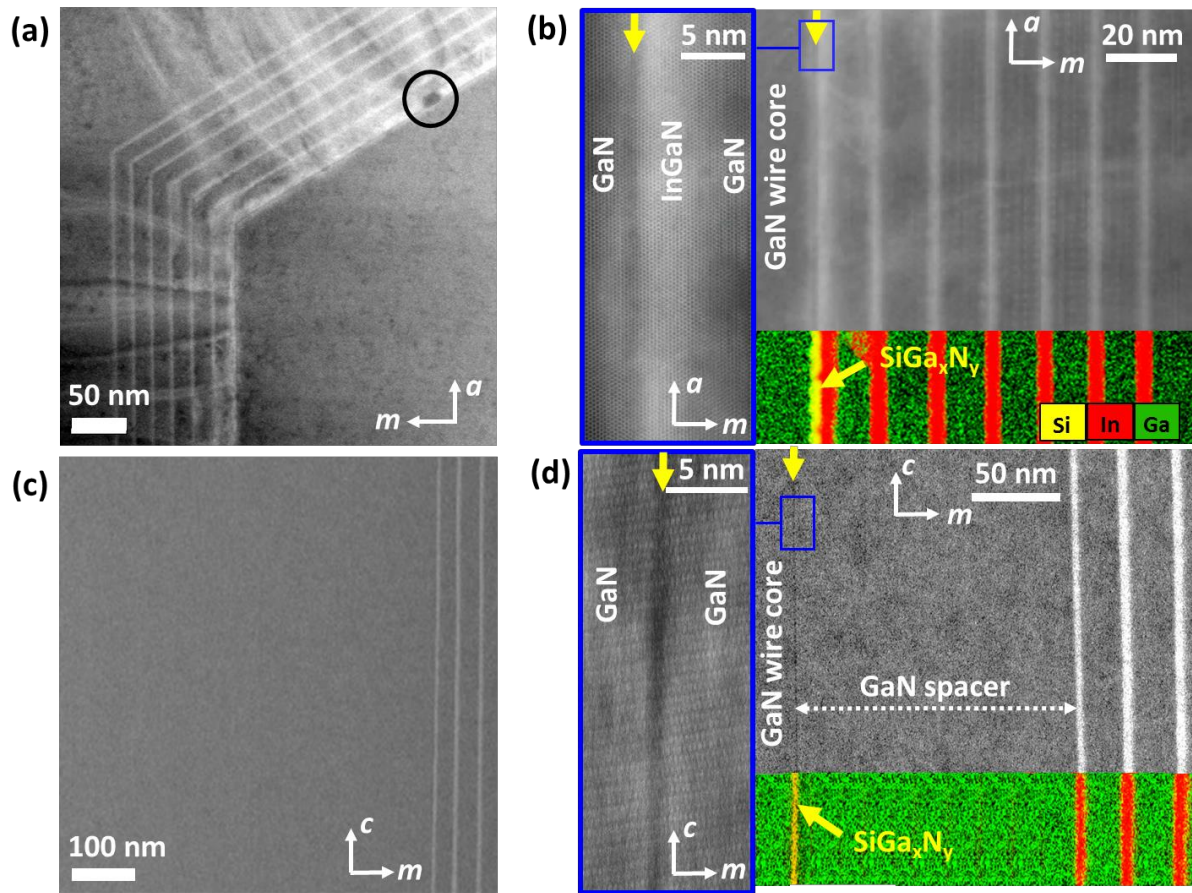


Figure 5



## Table of Contents Graphic

